JEE Journal of Ecological Engineering

Journal of Ecological Engineering 2023, 24(12), 143–151
https://doi.org/10.12911/22998993/172919
ISSN 2299–8993, License CC-BY 4.0

Received: 2023.09.01
Accepted: 2023.10.21
Published: 2023.11.04

Catalytic Ozonation of Ponceau 4R Using Multifunctional Magnetic Biochar Prepared from Rubber Seed Shell

Authors: Hung Minh Nguyen[1,2], Tram Thi Bao Truong[1,2], Hong-Hue Thi Nguyen[1,2], Phong Thanh Tran[1,2], Tuyet-Mai Tran-Thuy[1,2], Long Quang Nguyen[1,2], Dung Van Nguyen[1,2*]

[1] Faculty of Chemical Engineering, Ho Chi Minh City University of Technology (HCMUT), 268 Ly Thuong Kiet Street, District 10, Ho Chi Minh City, Vietnam

[2] Vietnam National University Ho Chi Minh City, Linh Trung Ward, Thu Duc City, Ho Chi Minh City, Vietnam

* Corresponding author's e-mail: nvdung@hcmut.edu.vn

ABSTRACT

Herein, abundant and underutilized rubber seed shell (RSS) was valorized for one-pot production of multifunctional magnetic biochar (MBC) through one-pot $FeCl_3$ activation. Fe_3O_4 and Fe^0 crystals were formed in MBC, providing a saturation magnetization of 6.83 emu/g. In addition, the material had a specific surface area of 378 m^2/g and a total pore volume of 0.22 cm^3/g. MBC was subsequently explored for catalytic ozonation of Ponceau 4R (P4R). As a result, MBC enhanced P4R ozonation in a broad pH range of 3.0–9.0. At pH 5.8, the pseudo-first-order rate constant of P4R decolorization with MBC improved by 50% compared to that without MBC. Summarily, RSS-derived MBC is a potential catalyst for enhanced ozonation of Ponceau 4R thanks to its low cost, eco-friendliness, relative effectiveness, and magnetic separability.

Keywords: rubber seed shell, magnetic biochar, one-pot strategy, catalytic ozonation, Ponceau 4R.

INTRODUCTION

Rubber trees (*Hevea brasiliensis*) are extensively cultivated in tropical regions, primarily for latex tapping (Qi et al., 2016). As part of their life cycle, rubber trees produce seeds that eventually fall to the ground (Borhan et al., 2019). According to Bhattacharjee et al. (2021), the global production of rubber seeds in 2016 was estimated to be approximately $7.7 \cdot 10^9$ kg. This biomass is commonly collected for oil extraction, leading to the release of abundant rubber seed shells (RSS) as waste (Sun et al., 2010). There have been increasing efforts in recent years to reduce waste and promote sustainability. Thus, the valorization of RSS can contribute to a more sustainable and resource-efficient rubber industry.

Biochar is a versatile and sustainable material produced through the pyrolysis of organic materials such as wood, agricultural waste, and manure in a low-oxygen environment (Xiang et al., 2020; Niedziński et al., 2023). Its highly porous structure and functional groups are advantageous for water purification (Kujawska, 2023). Nevertheless, traditional separation of biochar from treated water is generally complex and costly (Yi et al., 2020). To be more convenient, a hybrid material called magnetic biochar (MBC) has been developed (Thines et al., 2017; Zhao et al., 2021). The composite material includes magnetic particles for its magnetic separation by external magnetic fields and a biochar support for the adsorption of pollutants (Li et al., 2020; Yi et al., 2020). To facilitate the preparation of MBC, direct $FeCl_3$ activation of biomass has been devised (Do et al., 2022). $FeCl_3$ is dispersed into biomass, and the resulting mixture is pyrolyzed into MBC. Despite the fact that the properties of MBC are highly dependent on biomass resources, little RSS-derived MBC has been reported in the published literature. In this investigation, RSS was utilized to increase selection for the fabrication of MBC from potential biomass resources.

As mentioned before, MBC is commonly used for adsorbing various inorganic and organic pollutants from wastewater (Qu et al., 2022; Nguyen et al., 2023). In those situations, magnetic particles such as Fe_3O_4 and Fe^0 just aid in magnetic separation. Recently, such reports have explored the catalytic performance of magnetic Fe-based particles in MBC (Feng et al., 2021). Typically, MBC has become an inexpensive and efficient catalyst for the degradation of different organic pollutants using common oxidizing agents like hydrogen peroxide and persulfate (Rong et al., 2019; Nguyen et al., 2023). Nevertheless, the use of MBC for catalytic ozonation is still limited. That is due to the fact that manganese-based materials are normally considered for effective catalytic ozonation (Wang et al., 2019; Tran-Thuy et al., 2023). However, excessive levels of Mn can pose health risks. WHO recommends a guideline value of 400 μg/L for Mn in drinking water (Frisbie et al., 2012). For a more eco-friendly process, non-toxic catalysts should be used. In this study, low-cost RSS-derived MBC was explored as a potential catalyst for ozonation over a broad pH range. Ponceau 4R (P4R), a synthetic azo dye used in various food and beverage products, was selected for the ozonation process. Its structure is shown in Figure 1.

MATERIALS AND METHODS

Materials

Rubber seed shells were collected from Binh Long town, Binh Phuoc province, Vietnam. The collected biomass underwent sequential rinsing steps, first with tap water and then with distilled water. Next, desiccation was carried out at 105 °C for 24 h. The dried material was milled and sieved to collect a particle size range of 0.25–0.50 mm. The resulting powder was then stored in a plastic bag for later use. All chemicals were utilized without extra purification.

One-pot preparation of MBC from RSS

First, 2.000 g of RSS and 0.400 g of $FeCl_3$ were added to distilled water. The mass ratio of $FeCl_3$/RSS was 0.2. The mixture was stirred at ambient temperature for 24 h, then further dried at 105 °C for another 24 h. After that, the solid was pyrolyzed at 600 °C within 2 h at a continuous N_2 flow rate of 200 mL/h. The resulting product underwent meticulous cleaning with distilled water to eliminate all water-soluble components. The remaining solid was then dried once again at 105 °C for 24 h to yield MBC. The material was put in a desiccator for further experiments. In addition, BC, a reference sample, was prepared by direct pyrolysis of RSS without $FeCl_3$ addition.

Characterization of MBC

The crystal structure of MBC was determined using an X-ray diffractometer (D8 Advance, Bruker). Fourier transform infrared (FTIR) spectroscopy was obtained using a TENSOR 27 spectrometer. Magnetic properties were investigated at room temperature using a vibration sample magnetometer (VSM). Scanning electron microscopy (SEM) images were captured using a FE-SEM Hitachi S-4800 instrument. Porous properties were studied by a NOVA 2200e surface area and pore size analyzer at 77 K. Prior to the measurement, MBC was degassed at 300 °C for 3 h. The total pore volume (V_{total}) was computed at P/P_o = 0.99. The specific surface area (S_{BET}) was determined using the Brunauer-Emmett-Teller (BET) equation. Lastly, the average pore size (d_{avg}) was computed from $4V_{total}/S_{BET}$.

Ozonation of Ponceau 4R catalyzed by MBC

The catalytic activity of MBC was investigated for the decolorization of Ponceau 4R by O_3 at ambient temperature (31 °C). The scheme of the ozonation system is illustrated in Figure 2. First, a glass flask containing 500 mL of P4R (50 mg/L) and 0.50 g/L of MBC was filled. The pH of the P4R solution, which was measured by a Hanna HI 2210 pH meter, was adjusted using solutions of H_2SO_4 (0.1 M) and NaOH (1.0 M). In order to closely reach equilibrium adsorption, the suspension was stirred for 10 min. Next, P4R decolorization was initiated by bubbling ozone-containing airflow (0.46 mmol/min) from a Vina VN3 Ozone Generator. At predetermined intervals, samples were collected, and MBC was removed using a magnet. Lastly, P4R concentrations were analyzed by a Spectronic Genesys 2 PC UV-Vis spectrophotometer at 508 nm. The P4R adsorption capacity and removal of MBC were computed as follows:

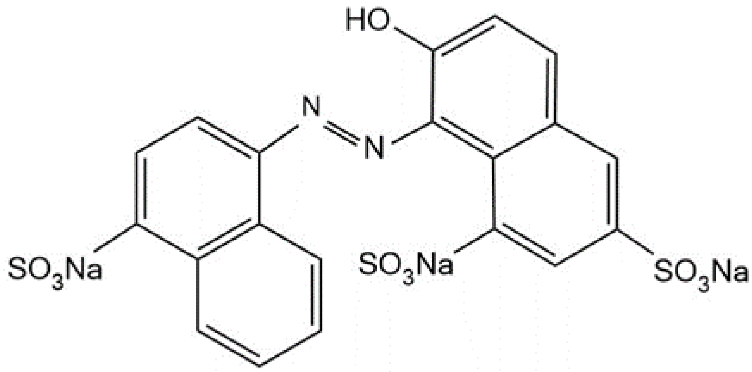

Figure 1. Structure of Ponceau 4R ($C_{20}H_{11}N_2Na_3O_{10}S_3$)

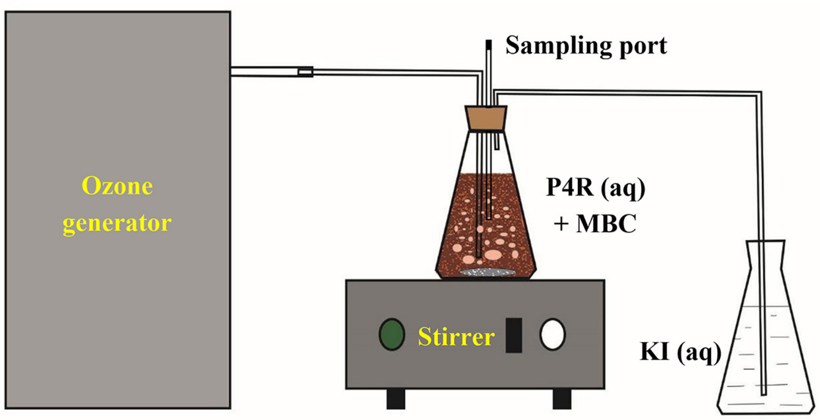

Figure 2. Scheme of the ozonation system

$$\text{Adsorption capacity (mg/g)} = \frac{C_0^A - C_{10}^A}{C_{MBC}} \quad (1)$$

$$\text{P4R removal (\%)} = \frac{C_0^O - C_{90}^O}{C_0^O} \times 100\% \quad (2)$$

For the adsorption step, C_0^A and C_{10}^A (mg/L) were the initial and 10-min P4R concentrations, respectively. Similarly, C_0^O and C_{90}^O (mg/L) represented the initial and 90-min P4R concentrations for the ozonation step, respectively. C_{MBC} (0.50 g/L) was MBC dosage. Furthermore, P4R decolorization was studied with the pseudo-first-order kinetic model. k (min^{-1}) represented the rate constant, while C_t^O (mg/L) was the P4R concentration after t (min) of decolorization.

$$k \times t = -\ln \frac{C_t^O}{C_0^O} \quad (3)$$

RESULTS AND DISCUSSION

Properties of MBC

Figure 3 depicts the X-ray diffraction (XRD) patterns of $FeCl_3$-loaded RSS and MBC. Prior to undergoing pyrolysis, the $FeCl_3$-loaded RSS exhibited a distinct peak at 2θ = 22.2°, indicating the presence of the (200) plane of cellulose from RSS. Hemicellulose and lignin, which are less ordered, could affect the baseline. Notably, the characteristic peaks of $FeCl_3$ were not detected in the mixture. $FeCl_3$ may exist in amorphous form, or the baseline may overlap its weak peaks. During the impregnation process, $FeCl_3$ electrolyte may disperse within the RSS structure rather than gather into big crystals. Regarding MBC, characteristic peaks at 2θ = 30.1, 35.4, 43.1, 53.3, 56.9, and 62.5° were attributed to the (220), (311), (400), (422), (511), and (440) planes of Fe_3O_4 crystal (JCPDS 19–0629), respectively. In addition, Fe^0 crystals were identified at 2θ = 44.8 and 60.6°, corresponding to (110) and (200) planes

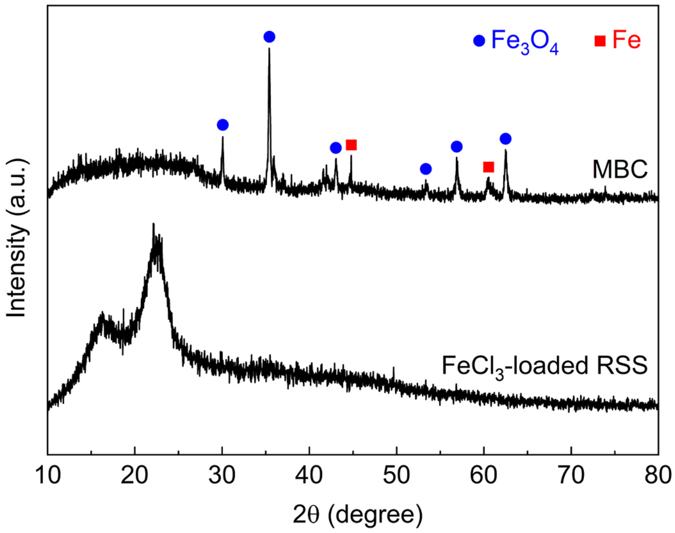

Figure 3. XRD patterns of $FeCl_3$-loaded RSS and MBC

(JCPDS 06–0696). Consequently, MBC contained both magnetic components, which have been described in a number of publications (Shin et al., 2021; Nguyen et al., 2023). The pathway for the formation of MBC during one-pot pyrolysis of $FeCl_3$-loaded RSS is proposed as follows:

$$RSS \rightarrow C, CO, H_2, H_2O \tag{4}$$

$$FeCl_3 \xrightarrow{+H_2O} FeO(OH) \rightarrow \\ \rightarrow Fe_2O_3 \xrightarrow{+C,CO,H_2} Fe_3O_4 \xrightarrow{+C,CO,H_2} Fe \tag{5}$$

First, pyrolysis of RSS could create porous carbon and gas-phase products like CO, H_2, and H_2O. Then, $FeCl_3$ could use the released H_2O to form FeO(OH). Consecutive reductions could not only produce Fe_3O_4 and Fe^0 particles but also activate porous carbon. As a result, S_{BET}, V_{total}, and d_{avg} of MBC reached 378 m^2/g, 0.22 cm^3/g, and 2.3 nm, respectively.

FTIR spectroscopy reveals distinct peaks from functional groups on the MBC surface (Figure 4). Typical groups were O-H (3839 and 3738 cm^{-1}), C-H (2919 and 2854 cm^{-1}), O=C=O (2351 cm^{-1}), C=O (1737 cm^{-1}), C=C (1530 cm^{-1}), and C-O (1147 cm^{-1}). Especially, the detected peak at 671 cm^{-1} may originate from C-Cl bonds, which may be formed from $FeCl_3$ activation of RSS (Devi et al., 2014; Xu et al., 2020; Tomin et al., 2022). More importantly, these functional groups could enhance the polarity of the MBC surface, thereby facilitating interactions with water-soluble organic pollutants present in aqueous environments.

As shown in Figure 5, MBC consisted of fragments of different shapes and sizes, which could be the result of fine milling and intensive pyrolysis. Additionally, it appears that few Fe-based particles were identifiable. Since $FeCl_3$ was well mixed with RSS before pyrolysis, it is likely that the Fe-based particles were trapped in the carbon matrix instead of just on the MBC surface (Bedia et al., 2017). This firm immobilization is anticipated to improve MBC stability during use.

As shown in Figure 6, MBC was completely attracted by a magnet. According to VSM analysis, the narrow hysteresis curve indicates that MBC can be magnetized and demagnetized with relative ease. The hysteresis loop displayed central symmetry, and the specific saturation magnetization reached 6.83 emu/g, indicating that magnetic components, including Fe_3O_4 and Fe^0 particles, were successfully loaded on the carbon matrix. Coercivity plays a vital role in determining whether to distinguish between soft and hard magnetic materials. According to Jiles (2003), the coercivity of the soft magnetic materials is 0.002–5 Oe, while that of the hard magnetic materials is 125 Oe–12 kOe. In this research, the coercivity of MBC was approximately 130 Oe, which was the hard magnetic material. Despite this, the weak coercivity of MBC could support effective magnetization and demagnetization by external magnetic fields.

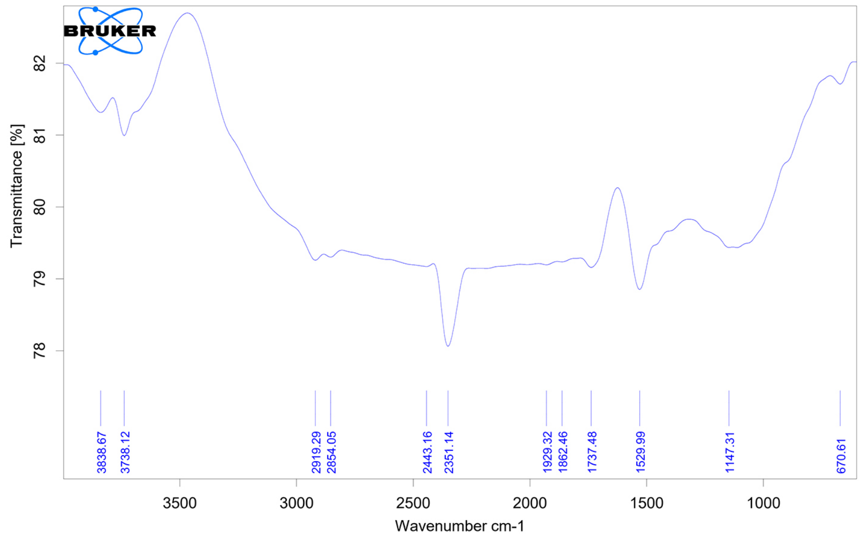

Figure 4. FTIR spectroscopy of MBC

Ozonation of Ponceau 4R catalyzed by MBC

Figure 7 shows that ozone, a strong oxidizing agent, decolorized 71% of P4R within 90 min of bubbling. When MBC was used, P4R was partly removed due to an adsorption capacity of 17 mg/g. In the subsequent ozonation step, P4R removal increased to 86%. The rate constants for ozonation of P4R without and with MBC were 0.014 min^{-1} (R^2 = 0.998) and 0.021 min^{-1} (R^2 = 0.993), respectively. Hence, the decolorization rate was improved by 50%. These results proved that MBC enhanced P4R removal by O_3. The suggested mechanisms for ozonation accelerated by Fe-based crystals in MBC (MBC–Fe) are as follows (Kishimoto et al., 2012; Ji et al., 2018; Yu et al., 2019):

$$MBC-Fe^0 + O_3 + 2H_2O \rightarrow MBC-Fe^{2+} + O_2 + 2OH^- \quad (6)$$

$$MBC-Fe^0 + 2O_3 \rightarrow MBC-Fe^{2+} + 2O_3^- \quad (7)$$

$$MBC-Fe^0 + O_3 + 2H^+ \rightarrow MBC-Fe^{2+} + O_2 + 2H_2O \quad (8)$$

$$MBC-Fe^{2+} + O_3 \rightarrow MBC-FeO^{2+} + O_2 \quad (9)$$

$$MBC-FeO^{2+} + H_2O \rightarrow MBC-Fe^{3+} + \bullet OH + OH^- \quad (10)$$

$$MBC-Fe^{3+} + O_3 + H_2O \rightarrow MBC-FeO^{2+} + \bullet OH + O_2 + H^+ \quad (11)$$

$$P4R + \bullet OH \rightarrow Intermediates \rightarrow Mineralization \quad (12)$$

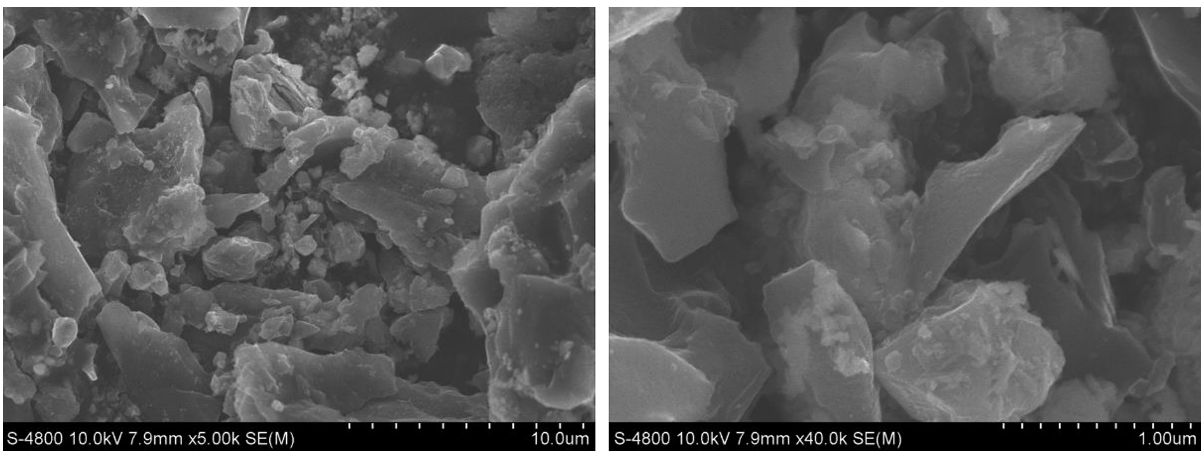

Figure 5. SEM images of MBC

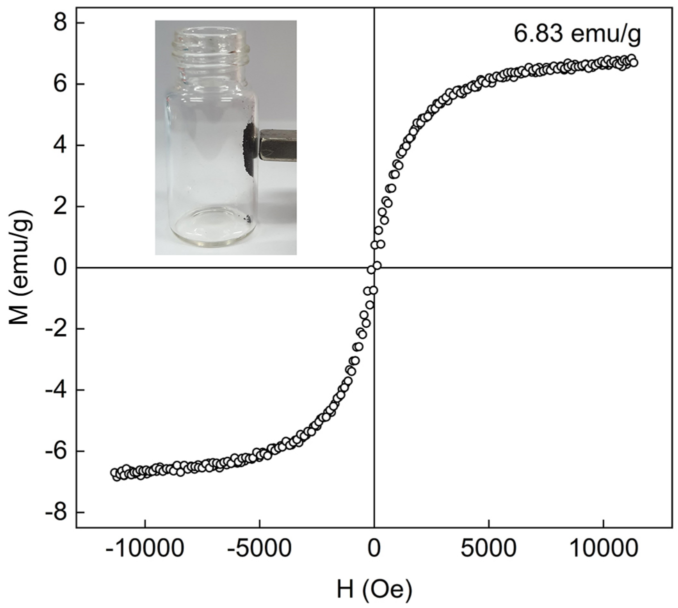

Figure 6. Hysteresis curve of MBC

MBC possessed both Fe^0 and $FeO.Fe_2O_3$ particles. Fe^0 was first converted into Fe^{2+} in a wide range of pH. In acidic media, Equation 8 can dominate, whereas neutral and basic media can boost Equations 6 and 7. Next, Fe^{2+} and Fe^{3+} sites might accelerate the formation of •OH radicals from O_3. Lastly, •OH could oxidize P4R. Although ozone itself can oxidize P4R directly, MBC could accelerate decolorization as well as reduce O_3 use.

The effect of pH on the ozonation of P4R with MBC is presented in Figure 8. In the adsorption step, the adsorption capacities of MBC at pH 3.0, 5.8, 8.0, and 10.0 were 20, 17, 14, and 13 mg/g, respectively. These results revealed a gradual decrease in adsorption capacity with increasing pH. In fact, the MBC surface with oxygen-containing functional groups might become more negative as pH increases. Therefore, its interaction with the anionic dye P4R may become weak. In the subsequent ozonation step, P4R decolorization was boosted with the increase in pH from 3.0 to 5.8. Next, similar decolorization rates were observed between pH 5.8 and 8.0. However, the decolorization rate was enhanced again in a basic environment at pH 10.0. In detail, the rate constants for ozonation of P4R at pH 3.0, 5.8, 8.0, and

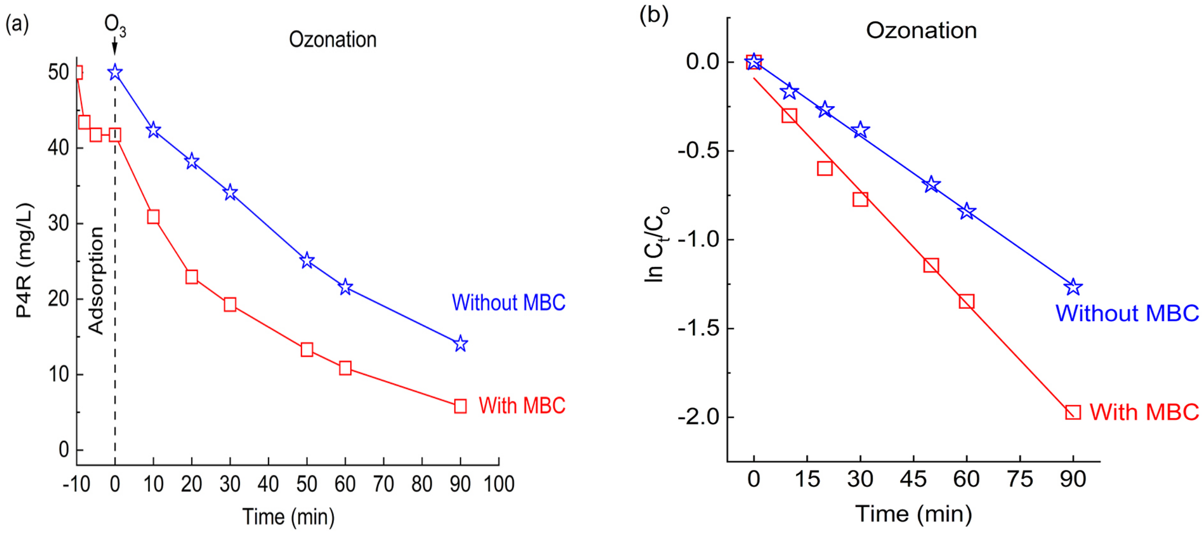

Figure 7. (a) Ozonation of P4R without and with MBC, and (b) its pseudo-first-order kinetics (pH 5.8, 50 mg/L P4R, 0.50 g/L catalyst).

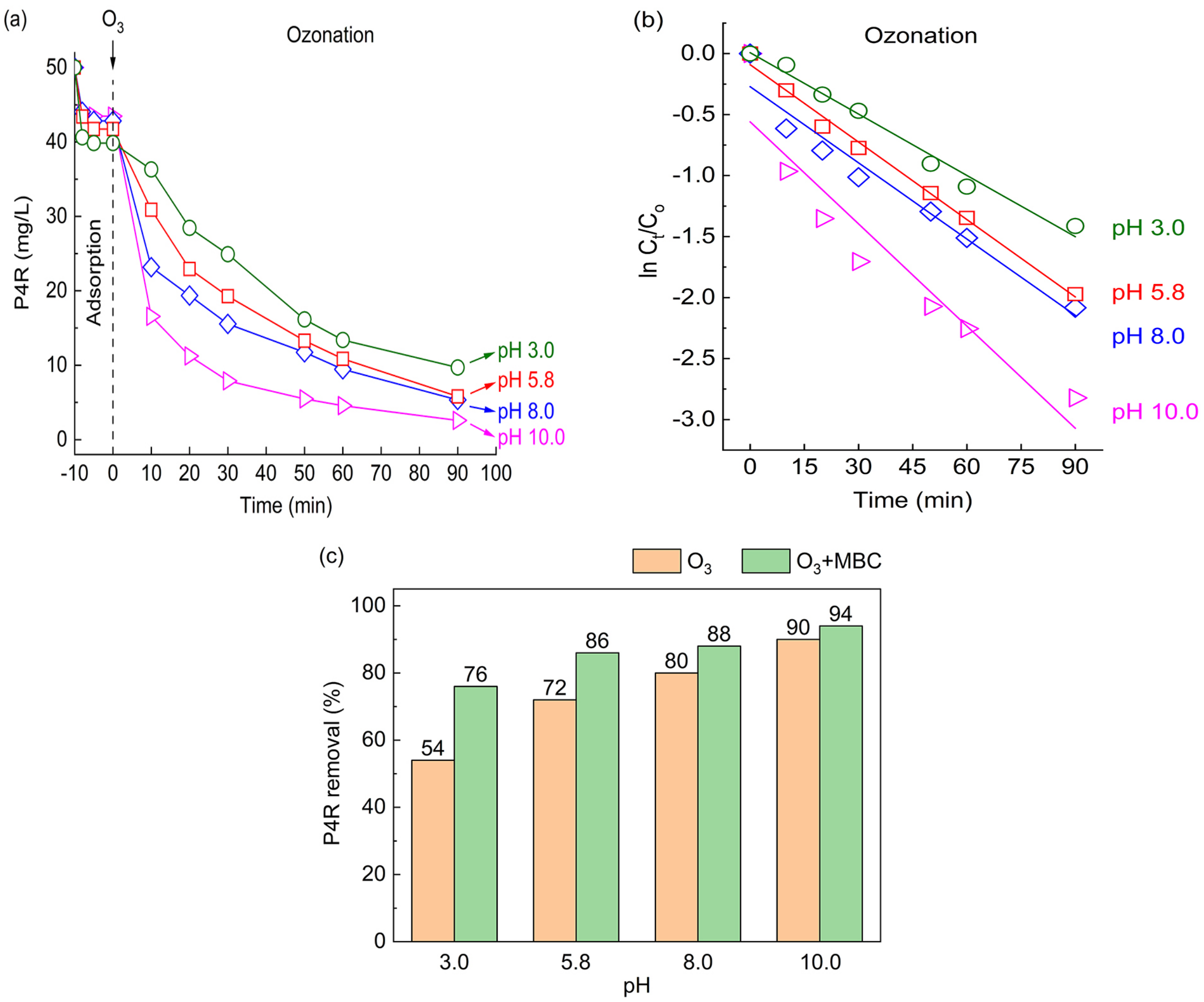

Figure 8. (a) Effect of pH on decolorization of P4R with O_3+MBC; (b) its pseudo-first-order kinetics; and (c) P4R removal at 90 min for O_3 alone and O_3+MBC (50 mg/L P4R, 0.50 g/L MBC).

10.0 were 0.017 min^{-1} (R^2 = 0.984), 0.021 min^{-1} (R^2 = 0.993), 0.020 min^{-1} (R^2 = 0.955), and 0.028 min^{-1} (R^2 = 0.893), respectively. To demonstrate the enhancement of MBC, P4R decolorization with O_3 alone as a reference was performed. As expected, P4R removal increased when pH rose (Figure 8c). Such reports demonstrate that indirect oxidation predominates at high pH (basic media), whereas direct ozonation prevails at low pH (acidic media), and both direct and indirect mechanisms operate at around neutral pH (Pera-Titus et al., 2004; Wang et al., 2020). As a result, non-catalytic ozonation occurred rapidly in basic environments, and MBC became less important. However, the weakness of direct non-catalytic ozonation at low pH emphasizes the importance of MBC catalyst. At pH 3.0, the presence of MBC improved P4R removal by 22%. Thus, low-cost MBC catalyst had potential for enhanced ozonation of P4R.

CONCLUSION

In this research, magnetic biochar was prepared from rubber seed shell and $FeCl_3$ via one-pot pyrolysis. MBC attained a S_{BET} of 378 m^2/g and a V_{total} of 0.22 cm^3/g as a result of activation. In addition, the formation of Fe_3O_4 and Fe^0 crystals resulted in the introduction of magnetic properties and catalytic activity for MBC. With a magnetic saturation of 6.83 emu/g, MBC is conveniently gathered by a magnet. Regarding its catalytic performance, MBC enhanced the ozonation of Ponceau 4R over a broad pH range. On the whole, rubber seed shell-derived magnetic biochar is a low-cost and effective catalyst for boosting the ozonation of Ponceau 4R.

Acknowledgement

We acknowledge Ho Chi Minh City University of Technology (HCMUT), VNU-HCM for supporting this study.

REFERENCES

1. Bedia, J., Monsalvo, V.M., Rodriguez, J.J. and Mohedano, A.F. 2017. Iron catalysts by chemical activation of sewage sludge with $FeCl_3$ for CWPO. Chemical Engineering Journal, 318, 224–230.
2. Bhattacharjee, A., Bhowmik, M., Paul, C., Das Chowdhury, B. and Debnath, B. 2021. Rubber tree seed utilization for green energy, revenue generation and sustainable development– A comprehensive review. Industrial Crops and Products, 174, 114186.
3. Borhan, A., Yusup, S., Lim, J.W. and Show, P.L. 2019. Characterization and modelling studies of activated carbon produced from rubber-seed shell using KOH for CO_2 adsorption. Processes, 7(11), 855.
4. Devi, P. and Saroha, A.K. 2014. Synthesis of the magnetic biochar composites for use as an adsorbent for the removal of pentachlorophenol from the effluent. Bioresource Technology, 169, 525–531.
5. Do, T.V.T., Bui, Q.L.N., Nguyen, H.M., Lam, H.H., Tran-Thuy, T.-M., Nguyen, L.Q., Ngo, D.T.H. and Nguyen, D.V. 2022. One-pot fabrication of magnetic biochar by $FeCl_3$-activation of lotus seedpod and its catalytic activity towards degradation of Orange G. Materials Research Express, 9, #105601.
6. Feng, Z., Yuan, R., Wang, F., Chen, Z., Zhou, B. and Chen, H. 2021. Preparation of magnetic biochar and its application in catalytic degradation of organic pollutants: A review. Science of The Total Environment, 765, #142673.
7. Frisbie, S.H., Mitchell, E.J., Dustin, H., Maynard, D.M. and Sarkar, B. 2012. World health organization discontinues its drinking-water guideline for manganese. Environmental Health Perspectives, 120(6), 775–778.
8. Ji, Y., Pan, Z., Yuan, D. and Lai, B. 2018. Advanced treatment of the antibiotic production wastewater by ozone/zero-valent iron process. CLEAN – Soil, Air, Water, 46(3), #1700666.
9. Jiles, D.C. 2003. Recent advances and future directions in magnetic materials. Acta Materialia, 51(19), 5907–5939.
10. Kishimoto, N. and Ueno, S. 2012. Catalytic effect of several iron species on ozonation. Journal of Water and Environment Technology, 10(2), 205–215.
11. Kujawska, J. 2023. Content of heavy metals in various biochar and assessment environmental risk. Journal of Ecological Engineering, 24(8), 287–295.
12. Li, X., Wang, C., Zhang, J., Liu, J., Liu, B. and Chen, G. 2020. Preparation and application of magnetic biochar in water treatment: A critical review. Science of The Total Environment, 711, #134847.
13. Nguyen, D.V., Nguyen, H.M., Bui, Q.L.N., Do, T.V.T., Lam, H.H., Tran-Thuy, T.-M. and Nguyen, L.Q. 2023. Magnetic activated carbon from $ZnCl_2$ and $FeCl_3$ coactivation of lotus seedpod: One-pot preparation, characterization, and catalytic activity towards robust degradation of acid orange 10. Bioinorganic Chemistry and Applications, 2023, #3848456.
14. Nguyen, H.M., Tran, A.T., Nguyen, D.N.L., Lam, H.H., Tran-Thuy, T.-M., Nguyen, L.Q., Le, T.X. and Nguyen, D.V. 2023. One-pot fabrication of zero-valent iron-embedded activated carbon from rosemary distillation residues for malachite green removal. Materials Research Express, 10(8), #085603.
15. Nguyen, L.T.K., Nguyen, L.Q., Nguyen, H.M., Nguyen, T.M., Lam, H.H., Tran-Thuy, T.-M. and Nguyen, D.V. 2023. Simple one-step synthesis of nipa frond-derived magnetic porous carbon for decolorization of acid yellow 23. Journal of Chemistry, 2023, #5447693.
16. Niedziński, T., Łabętowicz, J., Stępień, W. and Pęczek, T. 2023. Analysis of the use of biochar from organic waste pyrolysis in agriculture and environmental protection. Journal of Ecological Engineering, 24(4), 85–98.
17. Pera-Titus, M., García-Molina, V., Baños, M.A., Giménez, J. and Esplugas, S. 2004. Degradation of chlorophenols by means of advanced oxidation processes: a general review. Applied Catalysis B: Environmental, 47(4), 219–256.
18. Qi, D., Zhou, J., Xie, G. and Wu, Z. 2016. Optimizing tapping-tree density of rubber (Hevea brasiliensis) plantations in South China. Small-scale Forestry, 15(1), 61–72.
19. Qu, J., Shi, J., Wang, Y., Tong, H., Zhu, Y., Xu, L., Wang, Y., Zhang, B., Tao, Y., Dai, X., Zhang, H. and Zhang, Y. 2022. Applications of functionalized magnetic biochar in environmental remediation: A review. Journal of Hazardous Materials, 434, #128841.
20. Rong, X., Xie, M., Kong, L., Natarajan, V., Ma, L. and Zhan, J. 2019. The magnetic biochar derived from banana peels as a persulfate activator for organic contaminants degradation. Chemical Engineering Journal, 372, 294–303.
21. Shin, J., Lee, Y.-G., Kwak, J., Kim, S., Lee, S.-H., Park, Y., Lee, S.-D. and Chon, K. 2021. Adsorption of radioactive strontium by pristine and magnetic biochars derived from spent coffee grounds. Journal of Environmental Chemical Engineering, 9(2), #105119.
22. Sun, K. and Jiang, J.C. 2010. Preparation and characterization of activated carbon from rubber-seed shell by physical activation with steam. Biomass and Bioenergy, 34(4), 539–544.
23. Thines, K.R., Abdullah, E.C., Mubarak, N.M. and Ruthiraan, M. 2017. Synthesis of magnetic biochar from agricultural waste biomass to enhancing route for waste water and polymer application: A review. Renewable and Sustainable Energy Reviews, 67,

257–276.

24. Tomin, O. and Yazdani, M.R. 2022. Production and characterization of porous magnetic biochar: before and after phosphate adsorption insights. Journal of Porous Materials, 29(3), 849–859.
25. Tran-Thuy, T.-M., Tran, T.-P. and Nguyen, D.V. 2023. Cobalt-doped cryptomelane: Surface-tailored oxygen defects and efficiently catalytic ozonation of p-nitrophenol. Topics in Catalysis, 66(1), 289–296.
26. Wang, B., Zhang, H., Wang, F., Xiong, X., Tian, K., Sun, Y. and Yu, T. 2019. Application of heterogeneous catalytic ozonation for refractory organics in wastewater. Catalysts, 9(3), 241.
27. Wang, J. and Chen, H. 2020. Catalytic ozonation for water and wastewater treatment: Recent advances and perspective. Science of The Total Environment, 704, #135249.
28. Xiang, W., Zhang, X., Chen, J., Zou, W., He, F., Hu, X., Tsang, D.C.W., Ok, Y.S. and Gao, B. 2020. Biochar technology in wastewater treatment: A critical review. Chemosphere, 252, #126539.
29. Xu, Z., Zhou, Y., Sun, Z., Zhang, D., Huang, Y., Gu, S. and Chen, W. 2020. Understanding reactions and pore-forming mechanisms between waste cotton woven and $FeCl_3$ during the synthesis of magnetic activated carbon. Chemosphere, 241, #125120.
30. Yi, Y., Huang, Z., Lu, B., Xian, J., Tsang, E.P., Cheng, W., Fang, J. and Fang, Z. 2020. Magnetic biochar for environmental remediation: A review. Bioresource Technology, 298, #122468.
31. Yu, J., Xiao, K., Yang, J., Yu, W., Pei, K., Zhu, Y., Wang, J., Liang, S., Hu, J., Hou, H. and Liu, B. 2019. Enhanced sludge dewaterability and pathogen inactivation by synergistic effects of zero-valent iron and ozonation. ACS Sustainable Chemistry & Engineering, 7(1), 324–331.
32. Zhao, Q., Xu, T., Song, X., Nie, S., Choi, S.-E. and Si, C. 2021. Preparation and application in water treatment of magnetic biochar. Frontiers in Bioengineering and Biotechnology, 9, #769667.